Frontiers in Bioscience Landmark

Front. Biosci. (Landmark Ed) **2026**; 31(9): 52954
https://doi.org/10.31083/FBL52954

Original Research

Telomeric Replication Stress Promotes ALT-Associated Hallmarks in ATRX- and p53-Deficient Cells

Roberta Amato[1], Emanuela Micheli[1], Chiara Focaccetti[2], Roberto Bei[2], Piergiorgio La Rosa[3], Antonella Sgura[1,*], Francesco Berardinelli[1,4,*]

[1]Department of Science, University "Roma Tre", 00146 Rome, Italy
[2]Department of Clinical Sciences and Translational Medicine, Faculty of Medicine and Surgery, University of Rome "Tor Vergata", 00133 Rome, Italy
[3]Department of Neuroscience, Section of Human Anatomy, Catholic University of the Sacred Heart, 00168 Rome, Italy
[4]Laboratory of Neurodevelopment, Neurogenetics and Molecular Neurobiology Unit, IRCCS Santa Lucia Foundation, 00179 Rome, Italy
*Correspondence: antonella.sgura@uniroma3.it (Antonella Sgura); francesco.berardinelli@uniroma3.it (Francesco Berardinelli)
Academic Editor: Graham Pawelec
Submitted: 15 April 2026 Revised: 30 July 2026 Accepted: 18 August 2026 Published: 17 September 2026

Abstract

Background: Most human tumors maintain telomeres through telomerase activation; however, a subset relies on the telomerase-independent mechanism known as Alternative Lengthening of Telomeres (ALT). ALT-positive tumors are frequently characterized by inactivating alterations in ATRX (Alpha Thalassemia/Mental Retardation Syndrome X-linked) and p53 and by distinct molecular and cellular features. Although chronic telomeric replication stress has been proposed as a trigger for ALT, several aspects of this process remain poorly understood. Recent evidence suggests that ATRX depletion promotes the persistence of DNA secondary structures, including G-quadruplexes (G4), which can impair replication fork progression, leading to fork stalling and DNA damage. **Methods:** To investigate whether ATRX and p53 deficiency sensitize telomerase-positive cells to develop ALT-associated molecular features in response to telomeric replication stress, we analyzed telomeric DNA damage, telomere sister chromatid exchange (T-SCE), Telomeric Repeat-containing RNA (TERRA) expression, and C-circle formation in HCT116 cells proficient or deficient for ATRX and p53. ATRX was depleted using both transient (siRNA-mediated knockdown) and stable (shRNA-expressing clones) approaches, allowing us to distinguish the early cellular response from the features arising upon persistent ATRX loss. To further assess the contribution of telomeric replication stress, cells were treated with the G4-stabilizing ligand RHPS4. **Results:** Our data show that G4 stabilization, in the context of ATRX and/or p53 deficiency, promotes the appearance of multiple ALT-associated hallmarks, including telomeric DNA damage, increased T-SCE, and elevated TERRA expression. Moreover, the combined loss of ATRX and p53 permits cell-cycle progression despite the presence of RHPS4-induced telomeric replication stress and telomeric DNA damage. **Conclusions:** These findings clarify how ATRX and p53 loss, even in telomerase-positive cells, are permissive conditions for the emergence of ALT-associated hallmarks under telomeric replication stress and highlight the G2/M checkpoint as a critical barrier limiting the propagation of cells displaying these features.

Keywords: ALT; ATRX; G-quadruplex; telomeres; p53

1. Introduction

Telomeres are nucleoprotein complexes that protect the ends of linear chromosomes from being recognized as sites of DNA damage [1,2]. In humans, telomeric DNA consists of 10–15 kb of tandem TTAGGG repeats that end in a single-stranded 3′ overhang [3] bound by a complex of specialized proteins that regulate telomere homeostasis and contribute to genome stability. In somatic cells, telomeres shorten with each cell division, eventually leading to disruption of the protective telomeric structure [4] and driving cells toward senescence. Telomerase is the most important enzyme involved in telomere length maintenance. Indeed, most cancers (85–90%) maintain telomere length by upregulating the expression of this holoenzyme [5,6]. On the other hand, 10–15% of tumors utilize a telomeric recombination-based mechanism, called Alternative Lengthening of Telomeres (ALT), to maintain their telomeres [7,8]. ALT is prevalent in telomerase-negative cancers of mesenchymal and neural origin; however, it has also been proposed that telomerase-positive cancer cells may activate ALT as a resistance mechanism in response to anti-telomerase drugs [9]. The ALT mechanism showcases a series of recurring traits, yet it lacks a specific enzymatic function, rendering its inhibition notably challenging [10,11]. Specifically, ALT-positive tumors display cellular and molecular hallmarks including heterogeneous telomere length, Telomere Sister Chromatid Exchanges (T-SCE), Extra-Chromosomal Telomeric Repeat (ECTR) DNA, ALT-associated promyelocytic leukemia (PML) bodies (APBs) [12,13] and Telomeric Repeat-containing RNA (TERRA) [14]. In addition, ALT telomeres are characterized by chronic replication stress (RS) and DNA damage [15,16] principally caused by the abundant presence of non-canonical secondary structures such as R-loops and G-quadruplexes (G4) [17,18] that may interfere with DNA replication, leading to replication fork collapse and for-

mation of one-ended Double Strand Breaks (DSBs) [19]. Whole-genome sequencing studies have associated the induction of the ALT phenotype with loss-of-function mutations in components of the ATRX/DAXX/H3.3 complex [20,21,22].

ATRX is a member of the sucrose non-fermenting 2 (SNF2) family of chromatin-remodeling factors [23,24] and primarily works together with Death Domain-Associated Protein (DAXX) to mediate the deposition of the histone variant H3.3 at telomeric and pericentromeric chromatin [23,24,25].

Consistent with this function, ATRX appears to act as a suppressor of the ALT mechanism [26]. Although this protein does not possess a G4-unwinding activity, in the presence of non-canonical secondary structures, ATRX supports DNA replication by promoting their conversion into double-stranded DNA (dsDNA) owing to the deposition of histone H3.3 to maintain DNA in a B-form [20,27] and preventing DNA damage and replication stress resulting from fork stalling [28]. ATRX targets include tandem G-rich repeats capable of forming G4 structures [29,30].

Moreover, several studies have shown that the stabilization of G4 by G4-ligands increases homologous recombination (HR) at telomeres [18,31]. Despite its important role in ALT, ATRX mutation alone does not appear to be sufficient to trigger an ALT phenotype [21,22]. In ALT tumors, ATRX mutation often co-occurs with TP53 mutations [20,32,33,34] and TP53 is among the most frequently mutated genes in ALT cells [35,36].

Numerous studies demonstrate a function of p53 as a repressor of HR. Indeed, p53 localizes to stalled forks and physically interacts with the HR proteins RAD51 and RAD54, thereby inhibiting heteroduplex invasion [37] and favoring the processing of replication intermediates by facilitating their cleavage by resolvases [38]. Consistent with these findings, p53 is proposed as a suppressor of ALT activation; in fact, the p53 pathway is compromised in more than 80% of cell lines that use ALT as a Telomere Maintenance Mechanism (TMM) [39,40,41,42] even if the mutation of this pathway alone is not sufficient to establish an ALT phenotype [43].

Although mutations in ATRX and p53 are a genetic signature typical of ALT-positive cells, the relationship between the two proteins is, to date, not completely clear. In this context, we investigated the effect of p53 and ATRX depletion in ALT activation following telomeric RS induction. To this end, some of the features of the ALT mechanism (e.g., telomeric damage, T-SCE, TERRA expression, and C-circles) were analyzed in two isogenic colorectal cancer cell lines (HCT116 and HCT116 p53 –/–) transiently silenced for ATRX. In addition, to clarify the role of telomeric RS in the modulation of ALT markers, a well-known telomeric G4-ligand known for its ability to increase RS and telomeric DNA damage was used. Finally, to assess whether these ALT-associated features could be consolidated over time, we generated stable ATRX-depleted (shATRX) clones in both the p53-proficient and p53 –/– backgrounds and monitored the emergence of an ALT phenotype under persistent ATRX loss.

2. Materials and Methods

2.1 Cell Culture and Maintenance Conditions

HCT116 p53 +/+ and HCT116 p53 –/– isogenic human colon cancer cells (kindly provided by Prof. Alessandra Bisio, CIBIO, University of Trento) were cultured in Dulbecco's Modified Eagle's Medium (glucose 4.5 g/L) supplemented with 10% fetal bovine serum, 2 mM L-glutamine, 1 mM sodium pyruvate, and penicillin–streptomycin (100 U/mL and 100 µg/mL, respectively). The HCT116 p53 –/– line was generated in the laboratory of Professor Bert Vogelstein [44]; Phenotypic stability of these cell lines was confirmed by periodic Western blot analysis (**Supplementary Fig. 1A,B**). Telomerase activity (TA) was tested by TRAP assay, confirming that HCT116 p53 +/+ and HCT116 p53 –/– cells are telomerase-positive (**Supplementary Fig. 1C**). In addition, we performed a molecular cytogenetic karyotype characterization to verify that p53 +/+ and p53 –/– HCT116 cells were effectively two clones of the same tumor, differing by the p53 expression. It is worth noting that, as previously shown by Knutsen and coworkers, p53 –/– cells display an additional chromosomal rearrangement (t(5;7)(q13;p22)) when compared to the parental p53 +/+ cell line (**Supplementary Fig. 1D**) [45].

All cell lines were maintained at 37 °C in a humidified 5% CO_2 atmosphere and regularly screened for mycoplasma contamination.

2.2 Treatment Conditions

A stock solution of the pentacyclic acridine RHPS4 (3,11-difluoro-6,8,13-trimethyl-8H-quino [4,3,2-kl] acridinium methosulfate; Tocris, Bristol, UK) was prepared in dimethyl sulfoxide (DMSO).

HCT116 p53 +/+ and HCT116 p53 –/– were treated with the drug 24 h after plating, in accordance with the timing of the silencing protocol, and incubated for 72 h. Fresh working solutions were prepared from frozen aliquots for each experiment. Unless otherwise indicated, treatments were performed at the respective IC_{50} and IC_{30} values determined at 72 h (IC_{50} values: 3.5 and 6 µM for HCT116 p53 +/+ and HCT116 p53 –/–, respectively; IC_{30} values: 1.6 and 3.5 µM for HCT116 p53 +/+ and HCT116 p53 –/–, respectively).

2.3 Cell Proliferation and cPDL

Colorectal cancer cell lines were plated at a density of 7000 cells/cm^2 and exposed to RHPS4-containing medium. At the indicated time points (24, 48, 72, 96, and 120 h), cells were harvested and quantified. Cumulative population doublings (cPDL) were determined using the formula cPDL = $\log_2(N_f/N_0)$, where N_f represents the final cell number and

N_0 the initial number of plated cells. Data are representative of three independent experiments.

2.4 Sulforhodamine B (SRB) Assay

Exponentially growing cells were collected, counted, and seeded into 96-well plates at 2500 cells per well. This density was optimized to maintain exponential growth throughout the entire incubation time. The sulforhodamine B (SRB) assay was performed with minor modifications to the original protocol [46].

Briefly, cells were fixed with 10% ice-cold trichloroacetic acid for 1 h at 4 °C, followed by washing with deionized water. Cells were then stained with 0.057% SRB solution (Sigma-Aldrich, Co., St. Louis, MO, USA) (200 µL per well) for 30 min and washed four times with 1% acetic acid to remove unbound dye. After air-drying at room temperature, bound dye was solubilized in 10 mM unbuffered Tris base (200 µL per well). Absorbance was measured at 530 nm using a Victor X3 multilabel plate reader (PerkinElmer, Waltham, MA, USA). All experiments were performed in five independent replicates.

2.5 BrdU-Based Cell Cycle Analysis

48 h after RHPS4 treatment, cells were pulsed with 10 µM BrdU for 30 min and collected at 0, 8, and 12 h (Fig. 1C). Samples were fixed and permeabilized, and histones were removed by treatment with 2 M HCl, as previously described [47]. Incorporated BrdU was detected using an anti-BrdU primary antibody (1:100; DAKO, Glostrup, Denmark) followed by an Alexa Fluor 488-conjugated anti-mouse secondary antibody (1:100; Invitrogen, Carlsbad, CA, USA), each incubated for 1 h at room temperature in the dark. DNA content was evaluated by propidium iodide staining for biparametric analysis. Cell debris was excluded based on forward- and side-scatter parameters, and singlet cells were selected by pulse-geometry gating. BrdU-positive cells were then identified on BrdU fluorescence versus DNA-content plots, and their relative proportion was determined using CytExpert software (Beckman Coulter, Inc., San Diego, CA, USA).

2.6 ATRX siRNA

HCT116 p53 +/+ and p53 –/– were transfected with ATRX-targeted siRNAs to reduce the expression levels of this protein. The siATRX sequence used was the following: (ATRX #1: UUCCAUAGCCGUCUCAAGAUUCUCA) [48]. In addition, a siRNA scrambled sequence (siSCR: 5-GAUUGAAGACUGAUAUCACUU-3) [49] was transfected, as a control for nonspecific siRNA effects. Colorectal cancer cells were first transfected in suspension, with siRNA (Sigma-Aldrich, St. Louis, MO, USA) at a final concentration of 15 nM using Lipofectamine RNAiMAX (Thermo Fisher Scientific, Waltham, MA, USA). The medium was refreshed after 3 h. After 24 h from the first silencing, the cells, now in adhesion, were transfected again with 15 nM siRNA and Lipofectamine RNAiMAX. After 3 h, the culture medium was replaced with a medium containing RHPS4 at the concentrations corresponding to the respective IC_{30} and IC_{50}. After another 72 h of incubation, the cells were collected, and the silencing efficiency was verified by western blot and immunofluorescence. **Supplementary Fig. 2A** shows a schematic representation of the silencing protocol used. Western blot analysis (**Supplementary Fig. 2B,C**) showed that protein levels are unaffected by siSCR, whereas siRNA was capable of downregulating protein expression. In addition, it was also verified that RHPS4 treatment *per se* did not impact ATRX protein levels and ATRX silencing (**Supplementary Fig. 2D,E**). Finally, ATRX protein depletion was also confirmed by immunofluorescence (**Supplementary Fig. 2F**).

2.7 Lentiviral Production and Generation of Stable shATRX Clones

Lentiviral particles were produced in HEK293T cells using a second-generation packaging system. HEK293T cells were seeded at 3×10^6 cells per 10-cm dish and, the following day, co-transfected with 5 µg of the MISSION shRNA plasmid DNA targeting ATRX (Sigma-Aldrich, SHCLND-NM_000489), 3.75 µg psPAX2, and 1.25 µg pMD2.G (transfer:packaging:envelope ratio of 4:3:1). Transfection was performed with Lipofectamine 2000 (Invitrogen, cat.no. 11668019): the reagent was diluted in Opti-MEM and incubated for 5 min at room temperature, then combined with the plasmid DNA and incubated for a further 20 min to allow complex formation before being added dropwise to the cells. The medium was replaced 24 h after transfection, and viral supernatant was harvested once at 72 h post-transfection. The virus-containing medium was clarified by centrifugation at 500 × g for 10 min and filtered through a 0.45-µm filter. Target HCT116 p53 +/+ and p53 –/– cells were transduced in suspension by incubation with the filtered viral supernatant in the presence of polybrene (10 µg/mL) for 30 min at 37 °C, and then plated. A single round of transduction was performed. The medium was replaced the day after transduction, and puromycin selection was started the following day, at 1 µg/mL for one week followed by 0.5 µg/mL for a further week, until non-transduced control cells were completely eliminated.

Single-cell clones were isolated by limiting dilution: the selected bulk populations were serially diluted to approximately 1 cell/mL and seeded into 96-well plates at 200 µL per well; wells containing a single clone were identified by visual inspection and expanded under puromycin selection. ATRX knockdown was confirmed by Western blot, and clones were screened for ALT hallmarks as described. All the experiments on stable silenced clones were performed between passages 24 and 28 from transfection.

2.8 Western Blot

Cells were lysed in buffer containing 20 mM Tris-HCl (pH 7.5), 150 mM NaCl, 1 mM EDTA, 1% Triton X-100, and protease inhibitors. Equal amounts of protein (30 µg) were separated by SDS-PAGE and transferred onto polyvinylidene fluoride (PVDF) membranes (0.45 µm pore size; Immobilon-P, Millipore, Billerica, MA, USA). Membranes were blocked for 1 h at room temperature in 3% BSA and incubated overnight with primary antibodies against ATRX (rabbit polyclonal, 1:500 in 1% BSA; HPA001906, Sigma-Aldrich) and vinculin (mouse monoclonal, 1:10,000 in 3% BSA; V9131, Sigma-Aldrich) at 4 °C. After washing, membranes were incubated for 1 h at room temperature with HRP-conjugated goat anti-rabbit IgG (1:10,000; 1706515) and goat-anti-mouse IgG (1:10,000; 1706516) secondary antibodies (Bio-Rad Laboratories, Hercules, CA, USA). Protein signals were detected using an enhanced chemiluminescence system (ChemiDoc, Bio-Rad, Hercules, CA, USA). Experiments were performed at least three times, and band intensities were quantified using Image Lab software (Bio-Rad).

2.9 Metaphase and PCC Sample Preparation

Metaphase chromosome preparations were generated by treating cells with 5×10^{-6} M colchicine (Sigma-Aldrich) for 4 h to enrich for mitotic cells. Alternatively, premature chromosome condensation (PCC) in G2-phase cells was induced by a 30 min exposure to 50 nM calyculin A (Wako, Osaka, Japan). Chromosome spreads were prepared by incubating cells in hypotonic solution (75 mM KCl) for 20 min at 37 °C, followed by fixation in freshly prepared Carnoy's solution (methanol:acetic acid, 3:1 v/v). Fixed cells were then dropped onto glass slides, allowed to air-dry, and processed for subsequent cytogenetic analysis.

2.10 Chromosome Orientation–FISH (CO–FISH) Analysis

For CO-FISH analysis, cells were cultured in the presence of 5′-bromo-2′-deoxyuridine and 5-bromodeoxycytidine (BrdU/BrdC; Santa Cruz Biotechnology, Dallas, TX, USA) at a 3:1 ratio (final concentration 3×10^{-5} M) and were allowed to complete a single round of DNA replication overnight at 37 °C. Cells were subsequently collected, and chromosome spreads were generated as described above. CO-FISH was then performed as previously described [50] using strand-specific telomeric probes: a Cy3-labeled $(CCCTAA)_3$ probe and a FITC-labeled $(TTAGGG)_3$ probe (Panagene, Yuseong-gu, Korea). Images were acquired with a Zeiss Axio Imager M1 microscope equipped with a CCD camera. Telomere sister chromatid exchanges (T-SCEs) were scored only when both probe signals were clearly visible. For each condition, approximately 2500 chromosome ends were evaluated across three independent experiments. Telomere fragility was additionally assessed on the same images by scoring telomeric doublets, defined as either overlapping red and green signals or closely positioned signals of the two colors at individual chromosome ends.

2.11 Telomeric Quantitative Fluorescence In Situ Hybridization (Q-FISH)

Telomere length was assessed by Q-FISH on metaphase spreads. Chromosome preparations were left to age for two days, then washed in PBS and fixed in 4% formaldehyde for 2 min. After two further PBS rinses, slides were digested with pepsin for 10 min, washed, and dehydrated through an ethanol series. A Cy3-conjugated telomeric PNA probe combined with a chromosome 2 centromeric PNA probe (Panagene, Yuseong-gu, Korea) was applied to the slides; probe and target DNA were co-denatured at 80 °C for 3 min and left to hybridize for 2 h at room temperature in a humidified chamber. Following hybridization, slides underwent two 15-min washes in 70% formamide/10 mM Tris (pH 7.2)/0.1% BSA, then three 5-min washes in TBS (0.1 M Tris pH 7.5, 0.15 M NaCl) supplemented with 0.08% Tween-20. Slides were subsequently dehydrated through ethanol, air-dried, and counterstained with DAPI. Metaphases were acquired at 63× magnification on an Axio Imager.M1 microscope (Carl Zeiss, Jena, Germany), and telomeric signals were quantified with ISIS software (MetaSystems, Milano, Italy). For each telomere, length was measured as the ratio between its fluorescence intensity and that of the chromosome 2 centromere (T/C), used as an internal reference within every analyzed metaphase. Results are reported as T/C %. A minimum of 1000 chromosomes was scored per experimental point across two independent experiments.

2.12 TIF Co-Immunostaining

For immunofluorescence analysis, cells were processed by fixation in 4% paraformaldehyde at 4 °C, followed by permeabilization with 0.2% Triton X-100. Samples were blocked using 1% BSA at 37 °C. Co-detection of telomeric and DNA damage signals was carried out by overnight incubation at 4 °C with antibodies directed against TRF1 (rabbit polyclonal, Santa Cruz Biotechnology, Santa Cruz, CA, USA) and γH2AX (mouse monoclonal, Millipore Corp., Billerica, MA, USA). After washing in BSA 1%, cells were incubated with species-specific Alexa Fluor secondary antibodies (anti-rabbit 488 and anti-mouse 546; Invitrogen, Life Technologies, Carlsbad, CA, USA) for 1 h at 37 °C. Nuclear staining was performed with DAPI prior to image acquisition. Images were captured using a Zeiss Axio Imager M1 fluorescence microscope (Carl Zeiss, Jena, Germany) and analyzed with ISIS software (MetaSystems, Milano, Italy). Telomere-associated DNA damage was quantified by scoring co-localized TRF1/γH2AX foci in 300 nuclei per condition across three independent experiments.

2.13 PML Immuno-FISH for Detection of APBs

To detect APBs, cells were immunostained for PML with a mouse monoclonal antibody (E-11: sc-377390, Santa Cruz Biotechnology), following the procedure detailed above. Samples were subsequently rinsed for 5 min in PBS containing 0.05% Triton X-100 and probed for 1 h at room temperature with an Alexa Fluor 488–conjugated goat anti-mouse secondary antibody diluted in blocking solution. PML immunolabelling was followed by telomeric FISH, performed as described in the preceding section, to score PML–telomere colocalization. Imaging was carried out on an Axio Imager.M1 microscope (Carl Zeiss, Jena, Germany) equipped with a CCD camera, and colocalization events were quantified using ISIS software (MetaSystems, Milano, Italy). For each condition, at least 100 nuclei were examined across three independent experiments.

2.14 Telomeric RNA FISH

Telomeric RNA FISH was performed following previously published protocols [14,51] with minor modifications. Cells seeded on glass slides were first incubated for 30 s in ice-cold cytobuffer (100 mM NaCl, 300 mM sucrose, 3 mM $MgCl_2$, 10 mM PIPES, pH 6.8), followed by a 30 s extraction step in the same buffer supplemented with 0.5% Triton X-100. Cells were then fixed for 10 min at 4 °C in 4% paraformaldehyde. After fixation, samples were dehydrated through a graded ethanol series (70%, 85%, and 100%) and air-dried. Hybridization was carried out overnight at 37 °C using DNA probes at a final concentration of 0.5 pmol/µL in hybridization buffer containing 2× SSC, 2 mg/mL BSA, 10% dextran sulfate, and 50% deionized formamide.

Post-hybridization washes were performed as follows: three washes in 2× SSC/50% formamide at 39 °C for 5 min each, followed by three washes in 2× SSC at 39 °C for 5 min each, and a final wash in 2× SSC at room temperature for 5 min. Control oligonucleotides ($(TAACCC)_7$-Alexa488-3′ and $(AATCCC)_7$-Alexa488-3′; Integrated DNA Technologies, San Jose, CA, USA) were used as negative controls. As a control, samples were treated with RNase A (1 µg/µL, 1 h at 37 °C) prior to hybridization.

After hybridization, nuclei were stained with DAPI and coverslips were mounted in Vectashield mounting medium (Vector Laboratories, Burlingame, CA, USA). Fluorescence images were collected at 63× magnification with an Axio Imager M1 microscope (Carl Zeiss) equipped with a CCD camera, and image analysis was carried out using ISIS software (MetaSystems, Milano, Italy). All experiments were performed in at least three independent replicates.

2.15 C-circle Assay

C-circle assay was performed as previously described (Henson et al., 2017, [52]) with minor modifications. Total DNA was extracted using Quick C-Circle Lysis Buffer (50 mM KCl, 10 mM Tris HCl pH 8.5, 2 mM $MgCl_2$, 0.5% NP40, 0.5% Tween) and treated with 0.5 µg/µL protease (Qiagen, Hilden, Germany). Samples were placed in a thermomixer at 1400 rpm at 56 °C for 1 h, then 70 °C for 20 min. DNA less than 10 kilobases was enriched using the QiaQuick PCR purification kit (Qiagen). Samples, 100 ng in 10 µL each, were combined with 10 µL 0.2 mg/mL BSA, 10% Tween, 100 mM each dATP, dCTP, dGTP, and dTTP, 1× Φ29 buffer, and with or without 7.5 U Φ29 DNA polymerase (New England Biolabs (NEB), Ipswich, MA, USA) and incubated at 30 °C for 4 h, then 70 °C for 20 min. For quantification, the reaction products were dot-blotted onto a 2× SSC-soaked nylon positively charged membrane (GE Healthcare UK Limited, Little Chalfont, UK). DNA was UV–cross-linked onto the membrane, which was then hybridized with a 32P-labeled probe [T3AG2] in Church buffer (0.5 M phosphate buffer pH 7.2, 7% SDS, 1 mM EDTA, 0.1% BSA) overnight at 55 °C. The gel was washed twice and exposed to a PhosphorImager screen and analyzed by Quantity One software (Bio-Rad, Hercules, CA, USA). Signals of samples without Φ29 DNA polymerase were subtracted from signals obtained from corresponding samples with Φ29 DNA polymerase to determine the c-circle expression value.

2.16 Statistical Analysis

Statistical analyses were performed using GraphPad Prism version 10.5.0 (GraphPad Software, San Diego, CA, USA). Data are presented as mean ± SD or SEM from independent biological experiments, with technical replicates averaged before analysis; sample sizes are specified in the figure legends. Where indicated, values were normalized to the corresponding untreated control. Comparisons among multiple groups were performed using one- or two-way ANOVA followed by an appropriate multiple-comparisons test, whereas Student's *t*-test was used for comparisons between two groups. *p*-value ranges are always reported in figure legends, and $p < 0.05$ was considered statistically significant.

3. Results

3.1 p53 Status Modulates the Antiproliferative Response to RHPS4

To evaluate the influence of p53 on the antiproliferative response to RHPS4, colorectal cancer cells HCT116 p53 +/+ and the isogenic line p53 –/– were exposed to RHPS4 treatment for 72 h, at a concentration range from 0.5 to 8 µM. Analysis of the IC_{50} (compound concentrations required to achieve 50% inhibition of cell proliferation) showed that the effect of RHPS4 was influenced by the status of the p53 protein. The absence of p53 allowed cells to survive even at higher ligand concentrations (IC_{50} values: 3.5 and 6 µM for HCT116 p53 +/+ and HCT116 p53 –/–, respectively) (Fig. 1A). Interestingly, the IC_{50} of the p53 +/+ cell line corresponded to the IC_{30} (concentrations

of compound leading to 30% inhibition of cell proliferation) of the p53 –/– cell line (IC_{30} values: 1.6 and 3.5 µM for HCT116 p53 +/+ and HCT116 p53 –/–, respectively) (Fig. 1A). Therefore, subsequent experiments were carried out using iso-effect concentrations and thus, if not differently stated, cells were treated using their specific IC_{30} and/or IC_{50}. This design allows the two genotypes to be compared at equivalent levels of growth inhibition; in addition, the concentration of 3.5 µM represents an iso-molar condition, corresponding to the IC_{50} of p53 +/+ and the IC_{30} of p53 –/– cells, and therefore permits a direct comparison at an identical absolute dose.

The growth curves confirmed the higher sensitivity to treatment of the p53 proficient cell line (Fig. 1B). This observation is also supported by cell cycle analysis. Although RHPS4 induces a general slowing of progression along the cell cycle, the two cell lines showed a different response, especially in the progression through the S- and the G2/M-phase. After 8 h and 12 h from BrdU release, p53 +/+ cells treated with RHPS4 progressed slower through the S-phase and accumulated in the G2 phase. This effect was more pronounced in p53-proficient cells: at the iso-molar concentration of 3.5 µM, treatment increased the fraction of BrdU-positive cells in G2 in p53 +/+ cells at 8 h, whereas no such accumulation was observed in p53 –/– cells at the same absolute dose and time point (Fig. 1D,E).

3.2 Loss of p53 and ATRX exacerbates RHPS4-induced telomeric DNA damage

Secondary DNA structures that arise at chromosome ends are an obstacle for DNA replication, so their stabilization increases telomeric RS and consequently DNA damage [18,31]. In order to establish whether an increase of DSBs occurred at genomic and telomeric levels, γH2AX foci and their colocalizations with the component of the shelterin complex TRF1 were analyzed (Fig. 2A). Regardless of the p53 and ATRX status, no difference in basal genomic DNA damage (DNA damage outside telomeric regions) was observed (Fig. 2B). On the contrary, the G4 ligand treatment induced a dose-dependent increase of genomic damage, particularly when both p53 and ATRX were depleted (increase of 33 and 53% after IC_{30} and IC_{50} treatment, respectively) (Fig. 2C). Interestingly, basal levels of telomeric DNA damage were affected by the combined depletion of p53 and ATRX proteins (increase of 60%) (Fig. 2D). In agreement with previously published studies [47,53,54,55], treatment with RHPS4 resulted in a dose-dependent increase in telomeric damage across all conditions tested, with the largest increase (39%) observed in p53- and ATRX-double-depleted cells (Fig. 2E).

3.3 TERRA Transcription Increases Upon p53 and ATRX Depletion and Is Further Induced by RHPS4

To evaluate the levels of the telomeric transcript TERRA, which is a well-known ALT marker and is also induced after telomeric DNA damage, RNA-FISH was performed, and TERRA spots per nucleus were counted (Fig. 3A). An increase in telomeric transcripts was observed both in the absence of p53 and even more markedly when ATRX protein was silenced (2- and 3-fold increase, respectively). p53 and ATRX combined depletion caused a further slight increase in telomeric transcription (3.3-fold increase) (Fig. 3B). Moreover, RHPS4 was able to induce a 40% increase in this marker in p53-depleted cells. It is worth noting that the treatment induced only a slight increase in TERRA expression in p53 +/+ siATRX cells (29%), whereas this increase was even more pronounced when both proteins were non-functional (36%) (Fig. 3C).

3.4 p53 Restricts the Mitotic Entry of Cells Harboring Telomeric Doublets

In addition, ALT-positive cells are known to be characterized by the persistence of RS at telomeres, in part due to the presence of non-canonical secondary structures such as G4 and R-loops [15,16,17]. To recapitulate this condition, we stabilized telomeric G4 structures with the well-characterized G4 ligand RHPS4, which we and others have previously shown to increase telomeric RS [18,31].

To evaluate whether the telomeric DNA damage was due to an increase in RS, the frequency of telomeric doublets (TD) was assessed. Because RS-associated telomeric aberrations arise in S/G2 but may be resolved or eliminated before mitotic entry, TD and T-SCE were scored in two distinct cell-cycle windows: calyculin A-induced prematurely condensed G2 chromosomes, which capture cells before the G2/M transition, and colchicine-arrested metaphases, which capture only the cells that have successfully passed through it. Comparing these two windows allows us to distinguish the generation of telomeric aberrations from their transmission into mitosis. The G2 analysis was performed at the IC_{50} of each cell line only.

HCT116 p53 +/+ and p53 –/– cells transiently transfected with ATRX-targeted siRNA were treated with RHPS4, and the RS was examined. This analysis was performed by evaluating the frequency of multitelomeric fragile sites (or telomere doublets) observed after CO-FISH staining (Fig. 4A) both in G2- and M-phase of the cell cycle in order to evaluate the possible contribution of the G2/M cell cycle checkpoint.

In G2, silencing of ATRX alone caused a significant increase in the frequency of TD ($p = 0.023$) in the p53 +/+ condition. Treatment with RHPS4 induced a significant increase in telomeric doublets (58% and 39% increase in the presence and in the absence of ATRX, respectively), indicating that ATRX is not required for this effect (Fig. 4B,D). In p53 –/– cells, despite an increase in the frequency of doublets, no significant changes were detected (Fig. 4C,E).

In M-phase, treatment with the ligand induced a significant dose-dependent decrease of TD frequency in the p53 +/+ condition: comparing control and IC_{50}-treated

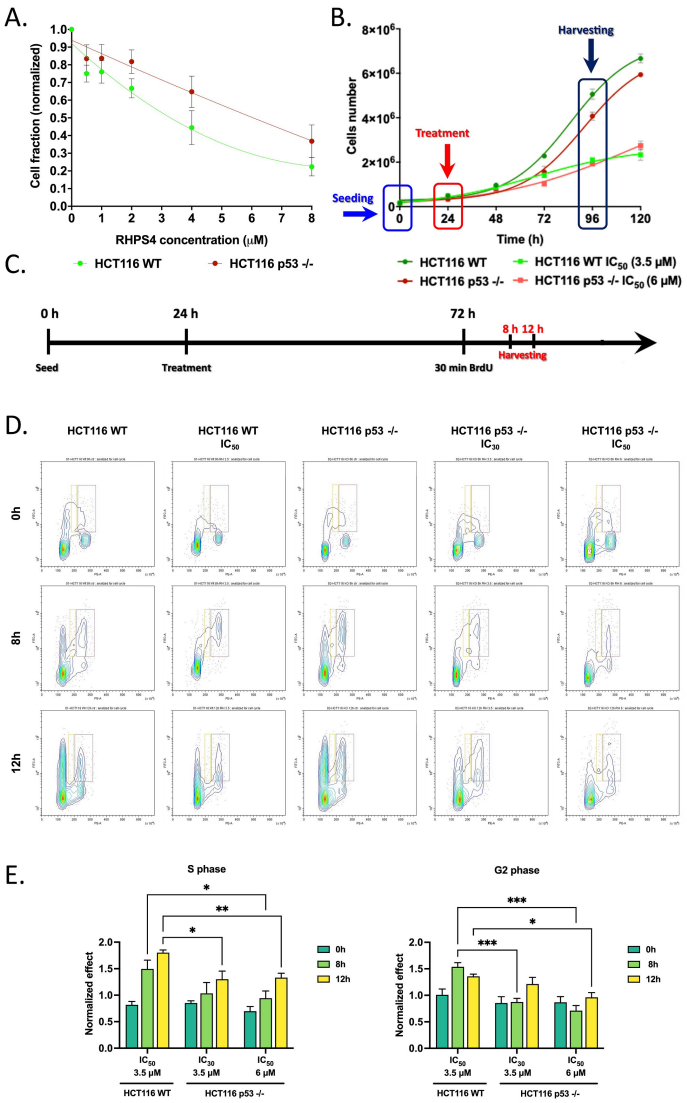

Fig. 1. RHPS4 induces p53-dependent growth inhibition and S/G2 cell-cycle delay in HCT116 cells. (A) The graphs show the proliferation rates of HCT116 p53 +/+ and p53 –/– 72 h following treatment with RHPS4 (from 0.5 to 8 μM) assessed by sulforhodamine B (SRB) assay. The data show a greater sensitivity to treatment when the p53 protein is proficient (IC_{50}: 3.5 and 6 μM in HCT116 p53 +/+ and p53 –/–, respectively). (B) Growth curves of HCT116 p53 +/+ and p53 –/– in the presence of RHPS4 treatment. Each cell line was treated with its respective IC_{50} and collected 24, 48, 72, 96, and 120 hours after seeding. Blue arrow indicates the seeding time, red arrow indicates the treatment time, and dark blue arrow indicates the harvesting time. (C) Timeline of experimental procedure for cell cycle characterization, (D) Cell cycle characterization performed using a 30 min BrdU pulse and chase approach in controls and RHPS4-treated samples. BrdU pulse was performed 48 hours after treatment with RHPS4 in order to follow BrdU-positive cells over the next 24 hours (fixing times: 0, 8, 12 h) (see the reported experimental timeline). Cell cycle profiles show the percentage of BrdU-positive and negative cells in the different phases of the cell cycle. Results were obtained from three independent experiments. (E) Quantification of the RHPS4-induced effect on S-phase and G2-phase progression, shown as the normalized effect at 0, 8, and 12 h after the BrdU pulse (see timeline in C). HCT116 WT were treated at their IC_{50} (3.5 μM), while HCT116 p53 –/– cells were analyzed both at their IC_{30} (3.5 μM matching the concentration used for WT) and at their own IC_{50} (6 μM). In the G2 phase, WT cells show a marked accumulation over time, whereas p53 –/– cells display a significantly lower accumulation (***$p < 0.001$; *$p < 0.05$), consistent with reduced G2/M checkpoint enforcement in the absence of p53. A comparable p53-dependent effect is seen in the S phase, where the treatment causes a milder delay in p53 –/– cells (*$p < 0.05$; **$p < 0.01$), indicating that the delay relies on functional p53. Data are mean ± SD of three independent experiments; statistical significance was assessed by two-way ANOVA with Tukey's multiple comparison test. p53, tumor protein 53; IC, half-maximal inhibitory concentration; RHPS4, G-quadruplex ligand; WT, G-quadruplex ligand.

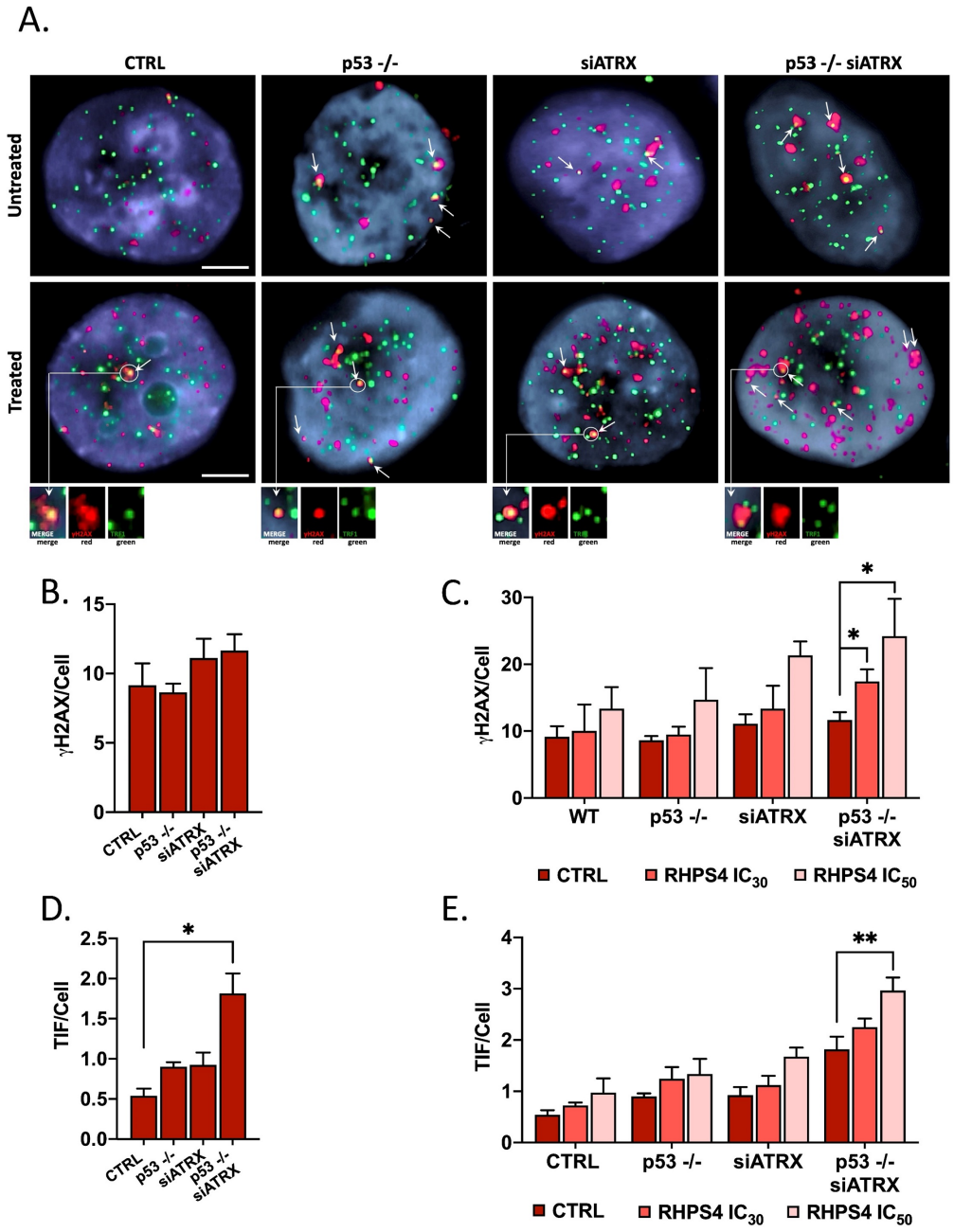

Fig. 2. p53 and ATRX modulate RHPS4-induced DNA damage at telomeres in HCT116 cells. (A) Representative images of Telomere dysfunction Induced Foci (TIFs) observed by γH2AX and TRF1 co-immunofluorescence staining for the colorectal cancer cell lines before and after RHPS4 treatment. For each cell line and condition, the single channels (γH2AX signals in red and TRF1 signals in green) and the merged images are reported. White arrows indicate γH2AX and TRF1 colocalizations. Scale bar, 8µm. (B) Frequency of total DNA damage in basal conditions (untreated samples). (C) Histogram of total DNA damage observed in HCT116 p53 +/+ and p53 –/– before and after siATRX or RHPS4 treatment (both at IC_{30} and IC_{50}) or under the combined action of the two conditions. The graph shows a significant increase in total DNA damage after treatment in the absence of both p53 and ATRX proteins. (D) Frequency of telomeric DNA damage in basal conditions (untreated samples). The graph shows a significant increase in telomeric damage in the absence of both p53 and ATRX proteins. Error bars denote standard errors of the mean (SEM). (E) Histogram of telomeric DNA damage observed in HCT116 p53 +/+ and p53 –/– before and after siATRX or RHPS4 treatment (both at IC_{30} and IC_{50}) or under the combined action of the two conditions. The graph shows a significant increase in telomeric DNA damage after treatment in all conditions evaluated. Statistical significance: $*p < 0.05$, $**p < 0.01$ (Student's *t*-test). γH2AX, phosphorylated histone H2AX; TRF1, telomeric repeat-binding factor 1; siATRX, siRNA targeting ATRX; ATRX, alpha-thalassemia/mental retardation, X-linked.

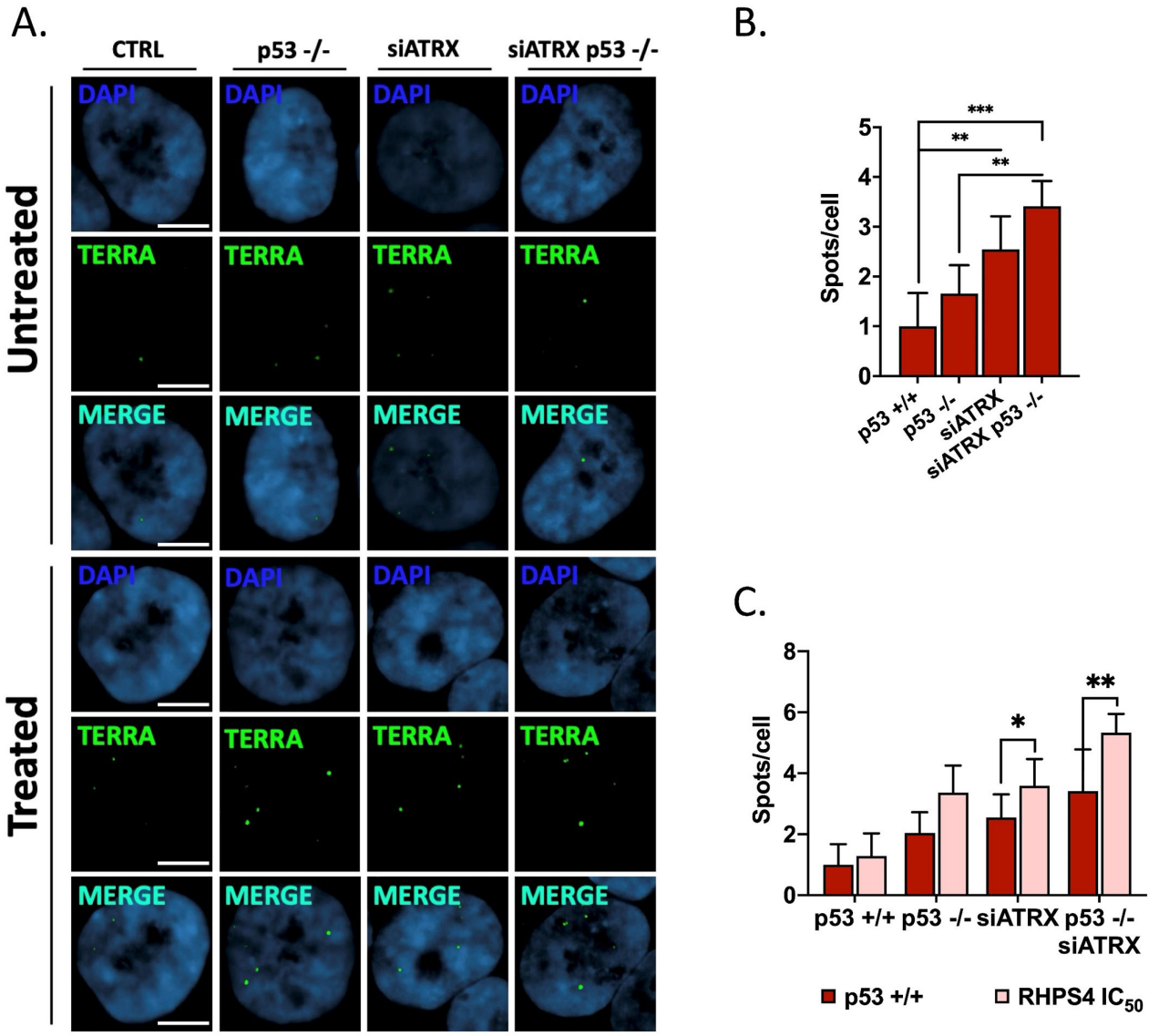

Fig. 3. p53 and ATRX modulate TERRA abundance and the response to RHPS4 in HCT116 cells. (A) Representative images of Telomeric Repeat-containing RNA (TERRA) spots observed by RNA-FISH. For each cell line and condition, the single channels (TERRA signals in green and nuclei in blue) and the merged images are reported. Scale bar, 8 µm. (B) Frequency of total telomeric transcript observed in all conditions without treatment. It can be noted an increase both in the absence of the p53 and ATRX proteins independently, and when both proteins are absent. (C) Histogram of telomeric transcript observed in HCT116 p53 +/+ and p53 –/– before and after siATRX or RHPS4 at IC_{50} treatment or under the combined action of the two conditions. Error bars represent standard deviations. Statistical significance: $*p < 0.05$, $**p < 0.01$, $***p < 0.001$ (Student's *t*-test). Experiments to evaluate the frequency of telomeric transcripts were repeated at least three times.

samples, a 61% decrease was observed in ATRX-proficient cells and a 32% decrease in ATRX-silenced cells (Fig. 4B,D). In p53 –/– cells, RHPS4 did not cause any change in ATRX-proficient cells, whereas when ATRX was silenced, a 33% increase was observed upon treatment (Fig. 4C,E).

The G2 and M data therefore point in opposite directions. In p53-proficient cells, RHPS4 increases telomere fragility in G2 but decreases it in M. Metaphase spreads only capture cells that have entered mitosis. We therefore interpret this decrease not as a reduction in telomeric RS, which is clearly induced, as shown by the G2 data and by the TIF analysis (Fig. 2), but as a result consistent with a p53-dependent checkpoint that holds back or eliminates the most damaged cells, which never reach mitosis. Two mechanisms could contribute: cells with unresolved telomeric RS may be arrested in G2, or the G2 arrest could give them time to complete replication at under-replicated telomeres and resolve fragile sites before mitosis. Both mechanisms

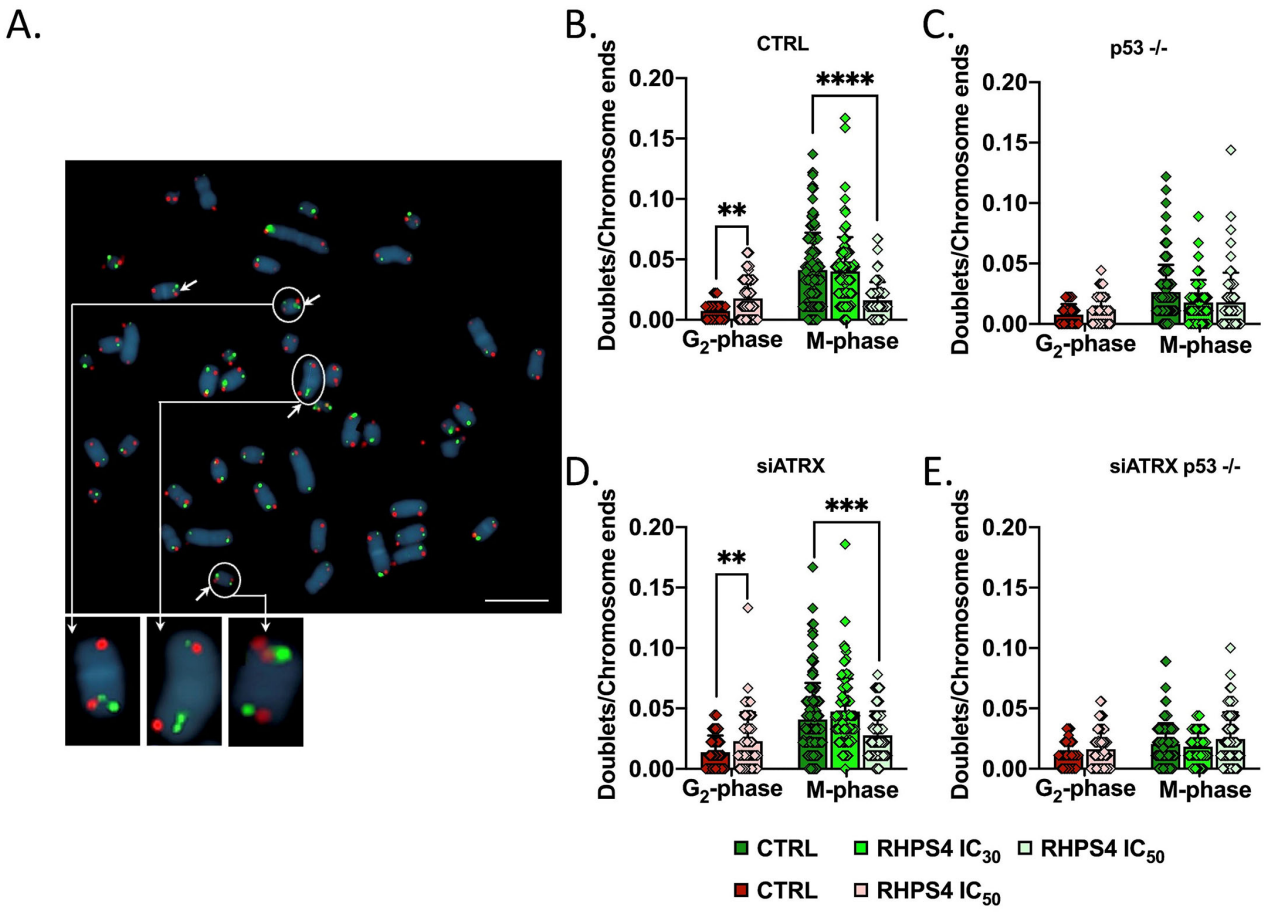

Fig. 4. p53 Limits the Mitotic Transmission of Telomere Doublets. (A) Representative metaphase spread stained by CO-FISH of colorectal cancer cells in which the telomeric doublets are highlighted and shown in the enlarged image. Scale bar, 5 µm. (B–E) Dotplots of double color doublets frequency in M- and G2- phases of HCT116 p53 +/+ and p53 –/– before and after siATRX or RHPS4 treatment (M-phase: IC_{30} and IC_{50}; G2 phase: IC_{50}) or under the combined conditions. Doublets analysis was performed across three independent experiments, with a minimum of 2500 chromosome ends evaluated for each cell line and condition. Telomere doublets, indicative of telomere fragility, were defined as either overlapping red and green signals or closely adjacent signals of the two colors at individual chromosome ends. Error bars represent standard deviations. Statistical significance: $^{**}p < 0.01$, $^{***}p < 0.001$, $^{****}p < 0.0001$ (Student's *t*-test). CO-FISH, chromosome orientation–FISH.

are consistent with the G2 accumulation and the greater sensitivity of p53 +/+ cells (Fig. 1).

3.5 p53 Prevents Damaged Cells From Entering Mitosis With T-SCE

To establish whether the previously observed changes were suggestive of telomeric recombination, T-SCE frequency was analyzed (Fig. 5). **In G2**, a significant increase in T-SCE was observed after treatment, independently of ATRX silencing (75% and 63% in p53 +/+ and p53 +/+ siATRX, respectively) (Fig. 5B,D). An increase in T-SCE was also found in the p53 –/– background, again independently of ATRX silencing (49% and 40% in p53 –/– and p53 –/– siATRX, respectively) (Fig. 5C,E).

In M-phase, p53 +/+ cells showed a dose-dependent decrease of T-SCE frequency upon treatment, which was significant in ATRX-silenced cells (49%) (Fig. 5B,D). Conversely, in p53 –/– cells, a significant increase in T-SCE was observed independently of ATRX silencing (69%, 66% and 74% in p53 –/– ATRX, siATRX IC_{30} and siATRX IC_{50}, respectively) (Fig. 5C,E).

T-SCE therefore mirrors the behaviour of telomeric doublets: recombination events are generated in G2 in both genetic backgrounds, but are transmitted into mitosis only when p53 is absent. Taken together, these data suggest that p53 does not prevent the generation of RHPS4-induced telomeric fragility and recombination but prevents their propagation through mitosis.

3.6 Transient ATRX Loss and p53 Depletion Induce ALT-Associated Features Without C-Circle Formation

Finally, we analyzed C-circles, one of the most specific ALT hallmarks. No changes were detected under any of the conditions tested: neither p53 loss, nor ATRX si-

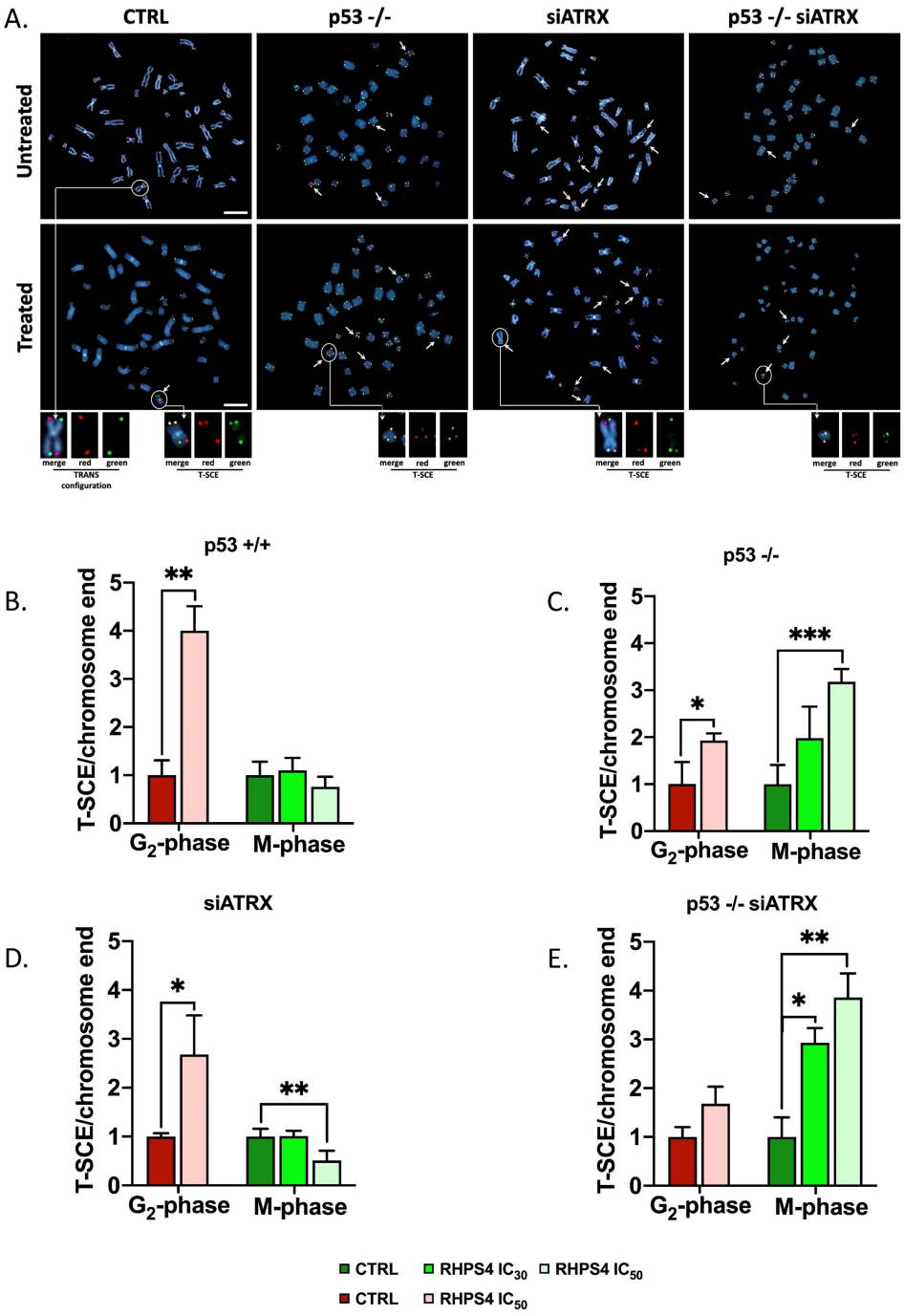

Fig. 5. p53 Limits the Mitotic Transmission of RHPS4-Induced Telomeric Recombination. (A) Representative metaphase spread stained by CO-FISH of HCT116 before and after treatment with RHPS4. Arrows indicate Telomere sister chromatid exchanges (T-SCE). For each cell line and condition, a representative chromosome with T-SCE is shown in the enlarged image. Scale bar, 5 µm. (B–E) Histograms of T-SCE frequency in M- and G2- phases of HCT116 p53 +/+ and p53 –/– before and after siATRX or RHPS4 treatment (M-phase: both at IC_{30} and IC_{50}; G2 phase: IC_{50}) or under the combined conditions. Each condition was normalized to its own control. The graphs show a significant increase in G2 telomeric recombination after treatment in the p53-proficient condition, both before and after ATRX silencing, and a slight increase in this marker in the p53 null condition, both before and after ATRX silencing. In M-phase, a significant increase after RHPS4 treatment can be observed only in the p53 null condition, both before and after ATRX silencing. Error bars represent standard deviations. Statistical significance: $*p < 0.05$, $**p < 0.01$, $***p < 0.001$ (Student's *t*-test). Analysis of telomere sister chromatid exchanges (T-SCEs) was conducted in three independent experiments, scoring a minimum of 2500 chromosome ends per condition.

lencing, nor their combination, nor RHPS4 treatment at either concentration affected C-circle levels (**Supplementary Fig. 3**). Thus, although transient depletion of p53 and ATRX, combined with G4 stabilization, elicited telomeric damage, TERRA induction and telomeric recombination, these changes were not accompanied by the appearance of C-circles, and are therefore better described as ALT-associated telomeric features than as a functionally engaged ALT phenotype. This prompted us to ask whether a persistent, rather than transient, loss of ATRX might be required for ALT initiation.

3.7 Persistent ATRX Loss Permits the Clonal Emergence of ALT Hallmarks, More Frequently in the Absence of p53

Taken together, the data described so far indicate that transient depletion of p53 and ATRX, combined with G4 stabilization, elicits several ALT-associated telomeric features but not C-circles, which are the most specific markers of ALT. Given the clonal and progressive nature of ALT, we generated stable ATRX-knockdown (shATRX) HCT116 p53 +/+ and p53 –/– lines (**Supplementary Fig. 4**), isolated single-cell clones, and assessed the cardinal ALT hallmarks (Fig. 6).

A modest C-circle signal was already detectable in the shATRX bulk populations, consistent with the presence of a small subpopulation of positive cells diluted within a largely negative background. Upon clonal isolation, however, C-circles became clearly evident in a subset of clones: 1/7 p53 +/+ (W clones; Fig. 6A,B) and 3/7 p53 –/– (A clones; Fig. 6C,D).

To determine whether C-circle positivity was accompanied by other cardinal ALT hallmarks, we next scored T-SCE frequency across representative shATRX clones (Fig. 7A). Notably, C-circle positivity did not invariably coincide with elevated telomeric recombination: the p53 +/+ clone W5 did not display a significant increase in T-SCE, whereas the p53 –/– clone A6 did. We therefore selected A6 (positive for both C-circles and T-SCE) for further characterization of the remaining ALT hallmarks.

Relative to the parental HCT116 p53 –/– line, the shATRX p53 –/– bulk population, and the C-circle-negative clone A4, which was itself indistinguishable from the parental control, A6 showed a significant increase in T-SCE frequency (Fig. 7A,B) and in APBs (Fig. 7C,D). A6 additionally displayed a higher number of TERRA foci (Fig. 7E) and brighter, more heterogeneous telomeric FISH signals, consistent with the telomere-length heterogeneity typical of ALT (Fig. 7F,G).

These data indicate that ALT emergence in this telomerase-proficient background is a rare, stochastic, and clonal event, undetectable at the population level and requiring persistent rather than transient ATRX loss. The higher proportion of C-circle-positive clones recovered in the p53-null background (3/7 vs 1/7) suggests that p53 restrains this process.

4. Discussion

In the present study, we investigated the interplay between ATRX and p53 in the cellular response to telomeric replication stress in a telomerase-positive background. To this end, telomerase-positive HCT116 p53 +/+ and p53 –/– colon cancer cells transiently depleted of ATRX were exposed to RHPS4, a telomeric G4 ligand used here to enhance telomeric replication stress and to model conditions resembling those observed in ALT tumor cells.

Our results showed that RHPS4 inhibited cell growth in both p53-proficient and p53-deficient HCT116 cells, in agreement with previous findings. Notably, during the first days after treatment, p53-deficient cells displayed a higher proliferation rate than their p53-proficient counterparts. This observation was supported by cell-cycle analysis, which revealed that p53 –/– cells were less sensitive to RHPS4 under the same treatment conditions, consistent with a reduced arrest at the G2/M boundary. These findings support the idea that p53 status influences the ability of cells to cope with RHPS4-induced stress and may facilitate the progression of damaged cells through the cell cycle. To assess the contribution of ATRX and p53 to genomic and telomeric DNA damage, both under basal conditions and following RHPS4 exposure, we performed γH2AX and TIF analyses. As expected, RHPS4 induced DNA damage not only at telomeres but also at the genomic level [56]. Genomic DNA damage increased in all cell lines after RHPS4 treatment, but the effect was more pronounced in ATRX-depleted and ATRX-depleted/p53 –/– cells, supporting a role for ATRX in limiting G4-associated replication stress and DNA damage [57,58,59]. This interpretation is in line with recent studies reporting activation of the ataxia-telangiectasia mutated (ATM)/checkpoint kinase 2 (CHK2)/p53 pathway [60] and altered p53 binding to chromatin in ATRX/DAXX-deficient cells following DNA damage [61].

Analysis of telomeric DNA damage further indicated that combined ATRX and p53 depletion caused a basal increase in telomere dysfunction, suggesting that both proteins contribute to telomere protection, in agreement with previous reports [32,33]. Our data indicate that depletion of either ATRX or p53 alone is sufficient to induce a mild increase in telomeric damage [61], whereas their combined loss has a stronger impact on telomere stability. Similarly, RHPS4-induced telomeric damage was enhanced in ATRX- and p53-deficient cells and was highest in double-depleted cells. This observation is consistent with the notion that, under replication stress, ATRX-deficient telomeres become more prone to fork collapse and DNA breakage, thereby promoting homology-directed repair pathways that are associated with ALT-related phenotypes [62,63]. ALT-positive cells lacking ATRX have been reported to display increased levels of TERRA, a telomeric lncRNA that enhances the recombinogenic potential of telomeres [48]. In addition, TERRA accumulation has been

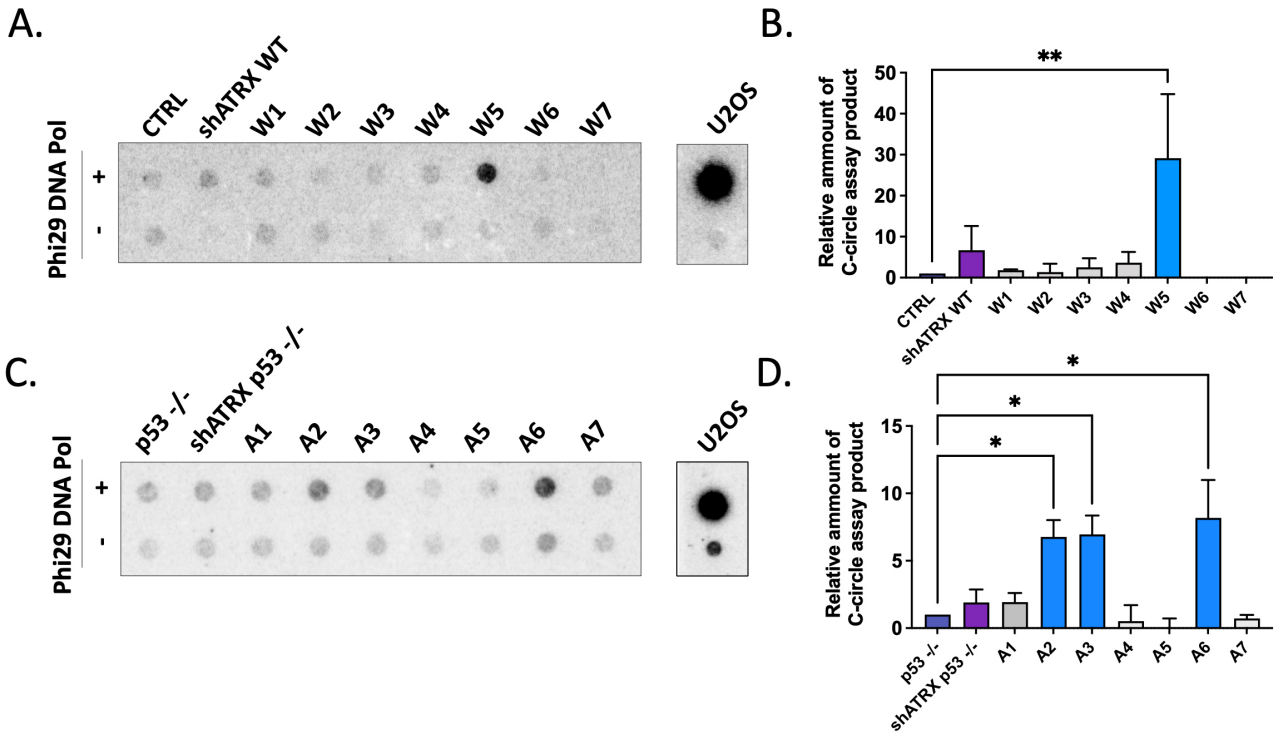

Fig. 6. p53 Loss Promotes C-Circle Formation Following Stable ATRX Depletion in HCT116 Cells. Stable ATRX-knockdown (shATRX) HCT116 p53 +/+ and p53 –/– lines were generated, and single-cell clones were isolated (W, p53 +/+-derived; A, p53 –/– -derived) and screened for C-circles, a cardinal ALT hallmark. The ALT-positive cell line U2OS was used as a positive control. (A) Representative C-circle assay of p53 +/+-derived (W) clones, performed in the presence (+) and absence (–) of Phi29 DNA polymerase, together with parental HCT116 (CTRL), the shATRX bulk population, and U2OS. (B) Quantification of the C-circle assay for W clones, expressed relative to parental control. Only clone W5 (blue) shows a clear C-circle signal. (C) Representative C-circle assay of p53 –/– -derived (A) clones, together with parental HCT116 p53 –/–, the shATRX p53 –/– bulk population, and U2OS. (D) Quantification of the C-circle assay for A clones, expressed relative to the parental control; C-circle-positive clones (A2, A3, and A6) are shown in blue. Clones were scored as C-circle-positive when the relative amount of C-circle assay product exceeded 3-fold that of the parental line. Error bars denote SEM; Statistical significance was assessed by one-way ANOVA followed by Dunnett's multiple comparison test. Only the comparisons relevant to the interpretation are shown. *$p < 0.05$; **$p < 0.01$.

associated with telomeric DNA damage in different cellular contexts [64,65,66]. In agreement with these observations, RNA FISH analysis revealed an increase in TERRA foci in ATRX-depleted cells, whereas p53 loss alone did not significantly affect TERRA levels. Notably, TERRA levels were further increased in cells lacking both ATRX and p53, suggesting that p53 loss may exacerbate the consequences of ATRX depletion, possibly by allowing the persistence of basal telomeric damage. RHPS4 treatment further increased TERRA expression in ATRX-depleted cells, reinforcing the connection between telomeric replication stress, ATRX loss, and TERRA upregulation. Despite the increase in telomeric DNA damage and TERRA expression, C-circles were not induced under any of the transient conditions tested (**Supplementary Fig. 3**). This result indicates that the alterations observed upon transient ATRX and p53 depletion, while recapitulating several ALT-associated features, do not lead to a functionally engaged ALT phenotype. A likely explanation is that ALT, being a clonal and progressive process, cannot be established within the short time window and transient conditions of siRNA-mediated depletion, and may require stable, long-term ATRX loss [67,68]

Taken together, the data obtained so far underscore the importance of p53 status in an ATRX-deficient background, particularly with regard to genomic and telomeric DNA damage and TERRA expression. In light of these findings, we hypothesized that one of the key functions of p53 in this context is to prevent the progression of damaged cells into mitosis. To test this possibility, we analyzed telomeric doublets (TDs) and T-SCEs in G2-condensed and mitotic chromosomes.

TD analysis, which is commonly used as a marker of telomeric replication stress, was performed to determine whether ATRX and p53 contribute to the control of the G2/M transition under telomeric stress conditions, although

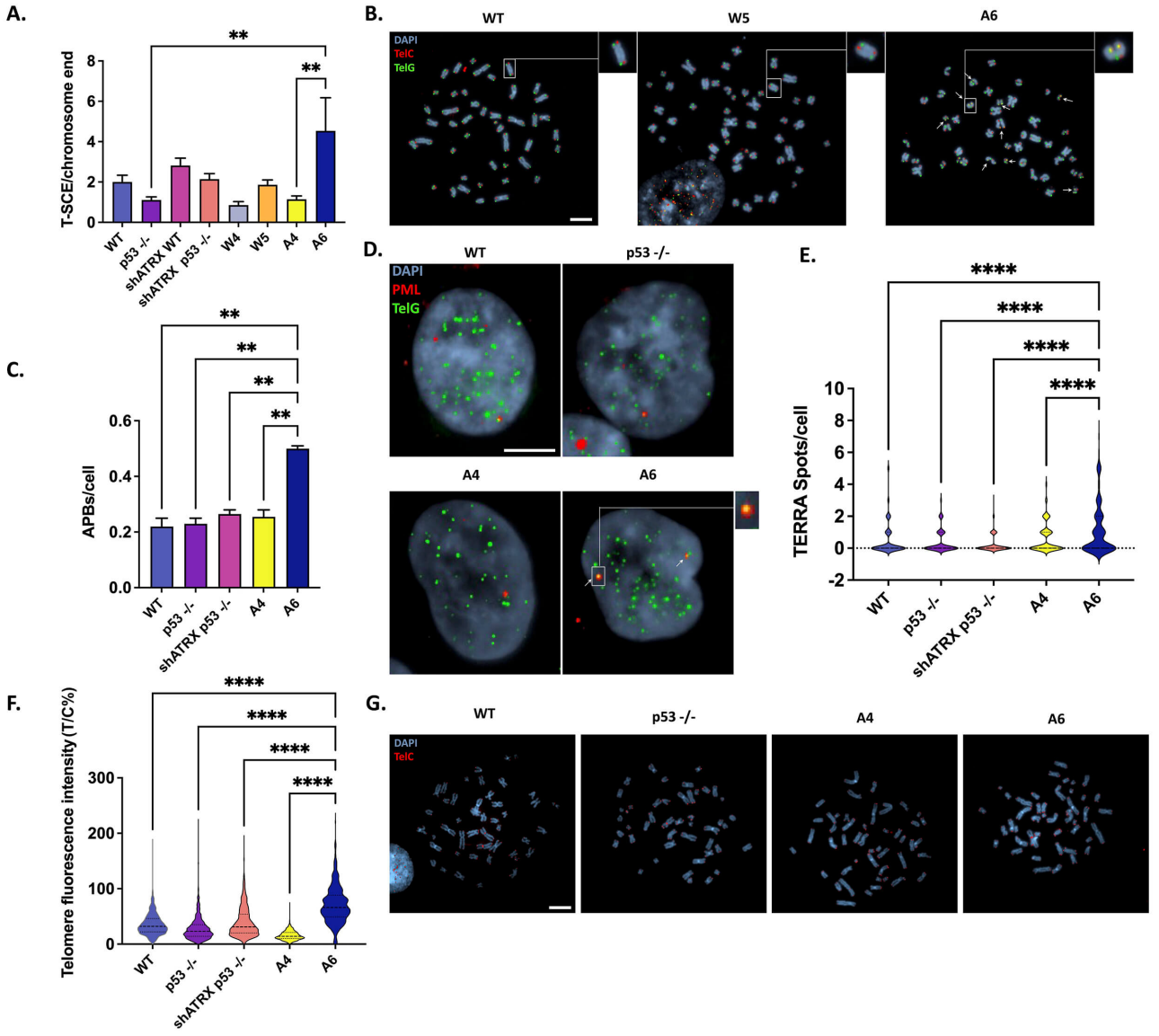

Fig. 7. The ATRX-Deficient, p53-Null HCT116 Clone A6 Exhibits Multiple ALT Hallmarks. (A) T-SCE frequency (events per chromosome end), scored by CO-FISH, across the indicated parental lines and shATRX clones (both p53 +/+/W and p53–/–/A series). Clone A6 shows a significant increase in T-SCE relative to the parental p53 –/– line and to clone A4 (**$p < 0.01$). (B) Representative CO-FISH metaphase spreads for WT, W5, and A6. Arrows indicate T-SCE events. Scale bar, 5 µm. (C) Quantification of ALT-associated PML bodies (APBs) per cell in the p53 –/– background. A6 displays a significant increase in APBs relative to the parental p53 –/– line, the shATRX p53 –/– bulk population, and clone A4 (**$p < 0.01$). (D) Representative immuno-FISH images of APB detection (PML in red, telomeres in green) for WT, p53 –/–, A4, and A6. The enlargement highlights a representative PML–telomere colocalization event (yellow). Scale bar, 8 µm. (E) Quantification of TERRA foci per cell in the p53 –/– background. A6 shows a significant increase in TERRA spots relative to the parental p53 –/– line, the shATRX p53 –/– bulk population, and clone A4 (****$p < 0.0001$). (F) Distribution of telomere fluorescence intensity (indicative of telomere length and heterogeneity). A6 exhibits brighter and more heterogeneous telomeric signals relative to the parental p53 –/– line, the shATRX p53 –/– bulk population, and clone A4 (****$p < 0.0001$), consistent with the telomere-length heterogeneity typical of ALT. (G) Representative telomere Q-FISH metaphase spreads (telomeres in red, DNA counterstained with DAPI) for WT, p53 –/–, A4, and A6. Scale bar, 5 µm.

the G2/M checkpoint is regulated by multiple pathways [69,70]. In G2-phase cells, ATRX silencing alone induced replication stress, as indicated by a significant increase in telomeric doublet frequency. RHPS4-mediated G4 stabilization further increased TD frequency in p53-proficient cells, independently of ATRX silencing, whereas this effect was not observed in p53-deficient cells.

In mitotic cells, by contrast, RHPS4 caused a dose-dependent reduction in TD frequency in p53-proficient backgrounds. Because metaphase preparations sample only cells that have entered mitosis, we interpret this reduction not as a decrease in telomeric replication stress, which is clearly induced, as shown by the G2 and TIF analyses, but as the consequence of a p53-dependent checkpoint that retains or eliminates the most damaged cells before mitotic entry. Consistently, p53-deficient cells, alone or combined with ATRX depletion, did not show this pattern, consistent with p53 loss permitting the escape of damaged cells from checkpoint control. To further investigate whether the cells progressing into mitosis under these conditions also displayed enhanced recombination at telomeres, we analyzed T-SCE frequency, one of the most reliable hallmarks associated with ALT. Interestingly, RHPS4 induced different outcomes depending on both cell-cycle phase and p53 status. In G2-phase cells, T-SCE frequency increased strongly in p53-proficient backgrounds, consistent with the accumulation of recombination-positive cells before mitotic entry. In M-phase cells, however, T-SCE frequency increased only in p53-deficient backgrounds, regardless of ATRX silencing, whereas p53-proficient mitotic cells showed a reduction. T-SCE thus mirrors the behavior of telomeric doublets: recombination events are generated in G2 in both backgrounds but are transmitted into mitosis mainly in the absence of p53. Overall, our findings support a model in which telomeric replication stress, particularly in the setting of ATRX depletion, generates ALT-associated telomeric recombination events, while p53 acts as a checkpoint-dependent barrier that would prevent their propagation through mitosis. We reasoned that, over time, this barrier should also influence whether such events become stably fixed. To test this directly, we moved from transient to stable ATRX loss: stable shATRX HCT116 p53 +/+ and p53 –/– lines were established, and single-cell clones were isolated and screened for the cardinal ALT hallmarks. In contrast to the transient conditions, persistent ATRX loss led to detectable C-circle formation only after single-cell cloning, with C-circle-positive clones occurring more frequently in the p53-deficient background (1/7 p53 +/+ clones versus 3/7 p53 –/– clones). No clear C-circle signal was detected in the corresponding bulk populations before clonal isolation. Among the p53 +/+ and p53 –/– clones, those displaying the highest C-circle levels were selected for further analysis of T-SCE frequency. Increased T-SCEs were observed only in the p53 –/– clone, which also exhibited other ALT-associated hallmarks, including elevated APBs and TERRA levels and greater telomere-length heterogeneity.

Together, these data indicate that the emergence of an ALT phenotype in a telomerase-proficient background is a rare, stochastic, and clonal event that requires persistent ATRX loss. The higher proportion of C-circle-positive clones recovered in the absence of p53 (3/7 versus 1/7) is consistent with the idea that p53 restricts the mitotic propagation of telomeric recombination events, thereby limiting their inheritance and accumulation over successive cell divisions and reducing the likelihood of ALT-positive clone emergence.

5. Limitations of the Study

This study presents limitations that should be considered when interpreting the findings. First, even if we used different derivative HCT116 cell lines to mimic p53 and ATRX genetic deficiency, our conclusions are based on a single telomerase-positive colorectal cancer parental model, and validation in additional cellular models and tumor types will be important to establish the generality of the proposed mechanism. Second, although the analysis of stable ATRX-depleted clones allowed us to capture rare ALT-associated phenotypes, the relatively small number of independent clones analyzed limits the statistical power to compare the frequency of ALT emergence between p53-proficient and p53-deficient backgrounds. Third, while our data support a model in which p53 prevents the transmission of unresolved telomeric lesions through mitosis, thereby reducing the opportunity for recombination-dependent telomere maintenance, we did not directly investigate the molecular mechanisms linking persistent telomeric damage to ALT establishment, such as break-induced replication. Future studies addressing these limitations will help define the additional genetic and epigenetic events that cooperate with ATRX and p53 loss to drive the emergence of a stable ALT phenotype.

6. Conclusions

Overall, our findings support a model in which sustained telomeric replication stress, particularly in the context of ATRX deficiency, promotes the emergence of ALT-associated phenotypes, while p53 acts as a critical barrier that restrains their evolution. Rather than functioning as a molecular switch that determines whether ALT is activated, p53 appears to be a factor that reduces the likelihood of ALT engagement by preventing cells carrying telomeric damage and recombination intermediates from progressing into mitosis. Over successive cell divisions, this checkpoint function limits the transmission of unresolved telomeric lesions to daughter cells. Because persistent telomeric DNA damage is thought to provide the substrate for break-induced replication and other recombination-dependent pathways that sustain ALT, this mechanism is likely to reduce the chance that rare cells gradually acquire a stable ALT phenotype. Consistent with this model, stable ATRX depletion generated ALT-associated clones only sporadically, with fully developed ALT features observed almost exclusively in the p53-deficient background. Taken together, our data suggest that p53 loss lowers the threshold for ALT emergence, supporting the view that ALT activation is a rare, stochastic, and multistep evolutionary process

that depends on additional cooperating genetic or epigenetic events. Identifying these factors will be important for understanding how ALT evolves during tumor progression and for anticipating potential mechanisms of resistance to telomerase-targeted therapies.

Availability of Data and Materials

The data that support the findings of this study are available from the corresponding authors upon reasonable request.

Author Contributions

RA and FB designed and performed siRNA experiments and analyzed the data. RA and FB designed and performed cytogenetic, immunofluorescence experiments and WB experiments and analyzed the data. RA and EM performed C-circles assay. CF and RB designed and performed cytofluorimetric analysis and analyzed the data. FB and AS conceived, initiated, and coordinated the project, designed and performed the experiments, analyzed data, and wrote the manuscript. RA, PLR, and EM contributed to the literature search and interpretation of the published evidence, participated in writing the manuscript, and critically reviewed and revised its content. All authors contributed to editorial changes in the manuscript. All authors read and approved the final manuscript. All authors have participated sufficiently in the work and agreed to be accountable for all aspects of the work.

Ethics Approval and Consent to Participate

Not applicable.

Acknowledgment

The authors gratefully acknowledge the BMCA PhD Program at the Department of Science, Roma Tre University, for providing the doctoral training environment in which RA conducted the research contributing to this study.

Funding

This study was supported by grants from Ateneo Roma Tre to F.B. and A.S. The Grant of Excellence Departments, MIUR (ARTICOLO 1, COMMI 314–337 LEGGE 232/2016) to Department of Science, University Roma Tre.

Conflicts of Interest

Given his role as an Editorial Board member, Roberto Bei had no involvement in the peer-review of this article and has no access to information regarding its peer review. Given their roles as Guest Editors, Piergiorgio La Rosa and Francesco Berardinelli had no involvement in the peer-review of this article and have no access to information regarding its peer review. Full responsibility for the editorial process for this article was delegated to Graham Pawelec.

Supplementary Material

Supplementary material associated with this article can be found, in the online version, at https://doi.org/10.31083/FBL52954.

References

[1] Blackburn EH. Telomere states and cell fates. Nature. 2000; 408: 53–56. https://doi.org/10.1038/35040500

[2] de Lange T. Shelterin: the protein complex that shapes and safeguards human telomeres. Genes & Development. 2005; 19: 2100–2110. https://doi.org/10.1101/gad.1346005

[3] Greider CW, Blackburn EH. Identification of a specific telomere terminal transferase activity in Tetrahymena extracts. Cell. 1985; 43: 405–413. https://doi.org/10.1016/0092-8674(85)90170-9

[4] Harley CB, Futcher AB, Greider CW. Telomeres shorten during ageing of human fibroblasts. Nature. 1990; 345: 458–460. https://doi.org/10.1038/345458a0

[5] Artandi SE, DePinho RA. Telomeres and telomerase in cancer. Carcinogenesis. 2010; 31: 9–18. https://doi.org/10.1093/carcin/bgp268

[6] Kim SH, Beausejour C, Davalos AR, Kaminker P, Heo SJ, Campisi J. TIN2 mediates functions of TRF2 at human telomeres. The Journal of Biological Chemistry. 2004; 279: 43799–43804. https://doi.org/10.1074/jbc.M408650200

[7] Cesare AJ, Reddel RR. Alternative lengthening of telomeres: models, mechanisms and implications. Nature Reviews. Genetics. 2010; 11: 319–330. https://doi.org/10.1038/nrg2763

[8] Episkopou H, Draskovic I, Van Beneden A, Tilman G, Mattiussi M, Gobin M, et al. Alternative Lengthening of Telomeres is characterized by reduced compaction of telomeric chromatin. Nucleic Acids Research. 2014; 42: 4391–4405. https://doi.org/10.1093/nar/gku114

[9] Al-Dulaimi S, Matta S, Slijepcevic P, Roberts T. 5-aza-2'-deoxycytidine induces telomere dysfunction in breast cancer cells. Biomedicine & Pharmacotherapy = Biomedecine & Pharmacotherapie. 2024; 178: 117173. https://doi.org/10.1016/j.biopha.2024.117173

[10] Apte MS, Cooper JP. Life and cancer without telomerase: ALT and other strategies for making sure ends (don't) meet. Critical Reviews in Biochemistry and Molecular Biology. 2017; 52: 57–73. https://doi.org/10.1080/10409238.2016.1260090

[11] Lee JJ, Lee J, Lee H. Alternative paths to telomere elongation. Seminars in Cell & Developmental Biology. 2021; 113: 88–96. https://doi.org/10.1016/j.semcdb.2020.11.003

[12] Yeager TR, Neumann AA, Englezou A, Huschtscha LI, Noble JR, Reddel RR. Telomerase-negative immortalized human cells contain a novel type of promyelocytic leukemia (PML) body. Cancer Research. 1999; 59: 4175–4179.

[13] Londoño-Vallejo JA, Der-Sarkissian H, Cazes L, Bacchetti S, Reddel RR. Alternative lengthening of telomeres is characterized by high rates of telomeric exchange. Cancer Research. 2004; 64: 2324–2327. https://doi.org/10.1158/0008-5472.can-03-4035

[14] Azzalin CM, Reichenbach P, Khoriauli L, Giulotto E, Lingner J. Telomeric repeat containing RNA and RNA surveillance factors at mammalian chromosome ends. Science (New York, N.Y.). 2007; 318: 798–801. https://doi.org/10.1126/science.1147182

[15] Dilley RL, Greenberg RA. ALTernative Telomere Maintenance and Cancer. Trends in Cancer. 2015; 1: 145–156. https://doi.org/10.1016/j.trecan.2015.07.007

[16] Sobinoff AP, Pickett HA. Alternative Lengthening of Telomeres: DNA Repair Pathways Converge. Trends in Genetics: TIG. 2017; 33: 921–932. https://doi.org/10.1016/j.tig.2017.09.003

[17] Arora R, Lee Y, Wischnewski H, Brun CM, Schwarz T, Azzalin CM. RNaseH1 regulates TERRA-telomeric DNA hybrids and telomere maintenance in ALT tumour cells. Nature Communications. 2014; 5: 5220. https://doi.org/10.1038/ncomms6220
[18] Amato R, Valenzuela M, Berardinelli F, Salvati E, Maresca C, Leone S, et al. G-quadruplex Stabilization Fuels the ALT Pathway in ALT-positive Osteosarcoma Cells. Genes. 2020; 11: 304. https://doi.org/10.3390/genes11030304
[19] Claussin C, Chang M. The many facets of homologous recombination at telomeres. Microbial Cell (Graz, Austria). 2015; 2: 308–321. https://doi.org/10.15698/mic2015.09.224
[20] Clynes D, Jelinska C, Xella B, Ayyub H, Scott C, Mitson M, et al. Suppression of the alternative lengthening of telomere pathway by the chromatin remodelling factor ATRX. Nature Communications. 2015; 6: 7538. https://doi.org/10.1038/ncomms8538
[21] Brosnan-Cashman JA, Yuan M, Graham MK, Rizzo AJ, Myers KM, Davis C, et al. ATRX loss induces multiple hallmarks of the alternative lengthening of telomeres (ALT) phenotype in human glioma cell lines in a cell line-specific manner. Plos One. 2018; 13: e0204159. https://doi.org/10.1371/journal.pone.0204159
[22] Li F, Deng Z, Zhang L, Wu C, Jin Y, Hwang I, et al. ATRX loss induces telomere dysfunction and necessitates induction of alternative lengthening of telomeres during human cell immortalization. The EMBO Journal. 2019; 38: e96659. https://doi.org/10.15252/embj.201796659
[23] Valenzuela M, Amato R, Sgura A, Antoccia A, Berardinelli F. The Multiple Facets of ATRX Protein. Cancers. 2021; 13: 2211. https://doi.org/10.3390/cancers13092211
[24] Drané P, Ouararhni K, Depaux A, Shuaib M, Hamiche A. The death-associated protein DAXX is a novel histone chaperone involved in the replication-independent deposition of H3.3. Genes & Development. 2010; 24: 1253–1265. https://doi.org/10.1101/gad.566910
[25] Lewis PW, Elsaesser SJ, Noh KM, Stadler SC, Allis CD. Daxx is an H3.3-specific histone chaperone and cooperates with ATRX in replication-independent chromatin assembly at telomeres. Proceedings of the National Academy of Sciences of the United States of America. 2010; 107: 14075–14080. https://doi.org/10.1073/pnas.1008850107
[26] Gaela VM, Hsia HY, Joseph NA, Tzeng WY, Ting PC, Shen YL, et al. Orphan nuclear receptors-induced ALT-associated PML bodies are targets for ALT inhibition. Nucleic Acids Research. 2024; 52: 6472–6489. https://doi.org/10.1093/nar/gkae389
[27] Clynes D, Jelinska C, Xella B, Ayyub H, Taylor S, Mitson M, et al. ATRX dysfunction induces replication defects in primary mouse cells. Plos One. 2014; 9: e92915. https://doi.org/10.1371/journal.pone.0092915
[28] Rizzo A, Salvati E, Porru M, D'Angelo C, Stevens MF, D'Incalci M, et al. Stabilization of quadruplex DNA perturbs telomere replication leading to the activation of an ATR-dependent ATM signaling pathway. Nucleic Acids Research. 2009; 37: 5353–5364. https://doi.org/10.1093/nar/gkp582
[29] Law MJ, Lower KM, Voon HPJ, Hughes JR, Garrick D, Viprakasit V, et al. ATR-X syndrome protein targets tandem repeats and influences allele-specific expression in a size-dependent manner. Cell. 2010; 143: 367–378. https://doi.org/10.1016/j.cell.2010.09.023
[30] Dharmaiah S, Malgulwar PB, Johnson WE, Chen BA, Sharin V, Whitfield BT, et al. G-quadruplex stabilizer CX-5461 effectively combines with radiotherapy to target α-thalassemia/mental retardation X-linked-deficient malignant glioma. Neuro-oncology. 2025; 27: 932–947. https://doi.org/10.1093/neuonc/noae248
[31] Min J, Wright WE, Shay JW. Alternative Lengthening of Telomeres Mediated by Mitotic DNA Synthesis Engages Break-Induced Replication Processes. Molecular and Cellular Biology. 2017; 37: e00226-17. https://doi.org/10.1128/MCB.00226-17
[32] Schwartzentruber J, Korshunov A, Liu XY, Jones DTW, Pfaff E, Jacob K, et al. Driver mutations in histone H3.3 and chromatin remodelling genes in paediatric glioblastoma. Nature. 2012; 482: 226–231. https://doi.org/10.1038/nature10833
[33] Watson LA, Goldberg H, Bérubé NG. Emerging roles of ATRX in cancer. Epigenomics. 2015; 7: 1365–1378. https://doi.org/10.2217/epi.15.82
[34] Cantero D, Mollejo M, Sepúlveda JM, D'Haene N, Gutiérrez-Guamán MJ, Rodríguez de Lope Á, et al. TP53, ATRX alterations, and low tumor mutation load feature IDH-wildtype giant cell glioblastoma despite exceptional ultra-mutated tumors. Neuro-oncology Advances. 2020; 2: vdz059. https://doi.org/10.1093/noajnl/vdz059
[35] MacKenzie D, Jr, Watters AK, To JT, Young MW, Muratori J, Wilkoff MH, et al. ALT Positivity in Human Cancers: Prevalence and Clinical Insights. Cancers. 2021; 13: 2384. https://doi.org/10.3390/cancers13102384
[36] Wang E, Rotondo F, Cusimano MD. Alpha thalassemia/mental retardation X-linked (ATRX) protein expression in human pituitary neuroendocrine tumours and its reported correlation to prognosis and clinical outcomes: A systematic review. Plos One. 2025; 20: e0313380. https://doi.org/10.1371/journal.pone.0313380
[37] Linke SP, Sengupta S, Khabie N, Jeffries BA, Buchhop S, Miska S, et al. p53 interacts with hRAD51 and hRAD54, and directly modulates homologous recombination. Cancer Research. 2003; 63: 2596–2605.
[38] Lee S, Cavallo L, Griffith J. Human p53 binds Holliday junctions strongly and facilitates their cleavage. The Journal of Biological Chemistry. 1997; 272: 7532–7539. https://doi.org/10.1074/jbc.272.11.7532
[39] Willers H, McCarthy EE, Alberti W, Dahm-Daphi J, Powell SN. Loss of wild-type p53 function is responsible for upregulated homologous recombination in immortal rodent fibroblasts. International Journal of Radiation Biology. 2000; 76: 1055–1062. https://doi.org/10.1080/09553000050111523
[40] Farooqi AS, Dagg RA, Choi LMR, Shay JW, Reynolds CP, Lau LMS. Alternative lengthening of telomeres in neuroblastoma cell lines is associated with a lack of MYCN genomic amplification and with p53 pathway aberrations. Journal of Neuro-oncology. 2014; 119: 17–26. https://doi.org/10.1007/s11060-014-1456-8
[41] Udroiu I, Marinaccio J, Sgura A. Inhibition of p53 and ATRX increases telomeric recombination in primary fibroblasts. FEBS Open Bio. 2023; 13: 1683–1698. https://doi.org/10.1002/2211-5463.13680
[42] Hartlieb SA, Sieverling L, Nadler-Holly M, Ziehm M, Toprak UH, Herrmann C, et al. Alternative lengthening of telomeres in childhood neuroblastoma from genome to proteome. Nature Communications. 2021; 12: 1269. https://doi.org/10.1038/s41467-021-21247-8
[43] Razak ZRA, Varkonyi RJ, Kulp-McEliece M, Caslini C, Testa JR, Murphy ME, et al. p53 differentially inhibits cell growth depending on the mechanism of telomere maintenance. Molecular and Cellular Biology. 2004; 24: 5967–5977. https://doi.org/10.1128/MCB.24.13.5967-5977.2004
[44] Bunz F, Dutriaux A, Lengauer C, Waldman T, Zhou S, Brown JP, et al. Requirement for p53 and p21 to sustain G2 arrest after DNA damage. Science (New York, N.Y.). 1998; 282: 1497–1501. https://doi.org/10.1126/science.282.5393.1497
[45] Knutsen T, Padilla-Nash HM, Wangsa D, Barenboim-Stapleton L, Camps J, McNeil N, et al. Definitive molecular cytogenetic characterization of 15 colorectal cancer cell lines. Genes, Chromosomes & Cancer. 2010; 49: 204–223. https://doi.org/10.1002/gcc.20730

[46] Vichai V, Kirtikara K. Sulforhodamine B colorimetric assay for cytotoxicity screening. Nature Protocols. 2006; 1: 1112–1116. https://doi.org/10.1038/nprot.2006.179
[47] Berardinelli F, Siteni S, Tanzarella C, Stevens MF, Sgura A, Antoccia A. The G-quadruplex-stabilising agent RHPS4 induces telomeric dysfunction and enhances radiosensitivity in glioblastoma cells. DNA Repair. 2015; 25: 104–115. https://doi.org/10.1016/j.dnarep.2014.10.009
[48] Flynn RL, Cox KE, Jeitany M, Wakimoto H, Bryll AR, Ganem NJ, et al. Alternative lengthening of telomeres renders cancer cells hypersensitive to ATR inhibitors. Science (New York, N.Y.). 2015; 347: 273–277. https://doi.org/10.1126/science.1257216
[49] Ritchie K, Seah C, Moulin J, Isaac C, Dick F, Bérubé NG. Loss of ATRX leads to chromosome cohesion and congression defects. The Journal of Cell Biology. 2008; 180: 315–324. https://doi.org/10.1083/jcb.200706083
[50] Berardinelli F, Antoccia A, Cherubini R, De Nadal V, Gerardi S, Cirrone GAP, et al. Transient activation of the ALT pathway in human primary fibroblasts exposed to high-LET radiation. Radiation Research. 2010; 174: 539–549. https://doi.org/10.1667/RR2127.1
[51] Montero JJ, López de Silanes I, Graña O, Blasco MA. Telomeric RNAs are essential to maintain telomeres. Nature Communications. 2016; 7: 12534. https://doi.org/10.1038/ncomms12534
[52] Henson JD, Lau LM, Koch S, Martin La Rotta N, Dagg RA, Reddel RR. The C-Circle Assay for alternative-lengthening-of-telomeres activity. Methods (San Diego, Calif.). 2017; 114: 74–84. https://doi.org/10.1016/j.ymeth.2016.08.016
[53] Salvati E, Leonetti C, Rizzo A, Scarsella M, Mottolese M, Galati R, et al. Telomere damage induced by the G-quadruplex ligand RHPS4 has an antitumor effect. The Journal of Clinical Investigation. 2007; 117: 3236–3247. https://doi.org/10.1172/JCI32461
[54] Berardinelli F, Sgura A, Facoetti A, Leone S, Vischioni B, Ciocca M, et al. The G-quadruplex-stabilizing ligand RHPS4 enhances sensitivity of U251MG glioblastoma cells to clinical carbon ion beams. The FEBS Journal. 2018; 285: 1226–1236. https://doi.org/10.1111/febs.14415
[55] Berardinelli F, Coluzzi E, Sgura A, Antoccia A. Targeting telomerase and telomeres to enhance ionizing radiation effects in in vitro and in vivo cancer models. Mutation Research. Reviews in Mutation Research. 2017; 773: 204–219. https://doi.org/10.1016/j.mrrev.2017.02.004
[56] Zizza P, Cingolani C, Artuso S, Salvati E, Rizzo A, D'Angelo C, et al. Intragenic G-quadruplex structure formed in the human CD133 and its biological and translational relevance. Nucleic Acids Research. 2016; 44: 1579–1590. https://doi.org/10.1093/nar/gkv1122
[57] Wang Y, Yang J, Wild AT, Wu WH, Shah R, Danussi C, et al. G-quadruplex DNA drives genomic instability and represents a targetable molecular abnormality in ATRX-deficient malignant glioma. Nature Communications. 2019; 10: 943. https://doi.org/10.1038/s41467-019-08905-8
[58] Watson LA, Solomon LA, Li JR, Jiang Y, Edwards M, Shinya K, et al. Atrx deficiency induces telomere dysfunction, endocrine defects, and reduced life span. The Journal of Clinical Investigation. 2013; 123: 2049–2063. https://doi.org/10.1172/JCI65634
[59] Pang Y, Cheng M, Wang J, Wang R, Chen X, Zhang C, et al. ATRX cooperates with TOP2B for replication fork stability and DNA damage response through G-quadruplex regulation. Nucleic Acids Research. 2025; 53: gkaf939. https://doi.org/10.1093/nar/gkaf939
[60] Akter J, Katai Y, Sultana P, Takenobu H, Haruta M, Sugino RP, et al. Loss of p53 suppresses replication stress-induced DNA damage in ATRX-deficient neuroblastoma. Oncogenesis. 2021; 10: 73. https://doi.org/10.1038/s41389-021-00363-6
[61] Gulve N, Su C, Deng Z, Soldan SS, Vladimirova O, Wickramasinghe J, et al. DAXX-ATRX regulation of p53 chromatin binding and DNA damage response. Nature Communications. 2022; 13: 5033. https://doi.org/10.1038/s41467-022-32680-8
[62] Lovejoy CA, Takai K, Huh MS, Picketts DJ, de Lange T. ATRX affects the repair of telomeric DSBs by promoting cohesion and a DAXX-dependent activity. Plos Biology. 2020; 18: e3000594. https://doi.org/10.1371/journal.pbio.3000594
[63] Aguilera P, López-Contreras AJ. ATRX, a guardian of chromatin. Trends in Genetics: TIG. 2023; 39: 505–519. https://doi.org/10.1016/j.tig.2023.02.009
[64] Porro A, Feuerhahn S, Lingner J. TERRA-reinforced association of LSD1 with MRE11 promotes processing of uncapped telomeres. Cell Reports. 2014; 6: 765–776. https://doi.org/10.1016/j.celrep.2014.01.022
[65] Porro A, Feuerhahn S, Delafontaine J, Riethman H, Rougemont J, Lingner J. Functional characterization of the TERRA transcriptome at damaged telomeres. Nature Communications. 2014; 5: 5379. https://doi.org/10.1038/ncomms6379
[66] Tutton S, Azzam GA, Stong N, Vladimirova O, Wiedmer A, Monteith JA, et al. Subtelomeric p53 binding prevents accumulation of DNA damage at human telomeres. The EMBO Journal. 2016; 35: 193–207. https://doi.org/10.15252/embj.201490880
[67] Graham MK, Kim J, Da J, Brosnan-Cashman JA, Rizzo A, Baena Del Valle JA, et al. Functional Loss of ATRX and TERC Activates Alternative Lengthening of Telomeres (ALT) in LAPC4 Prostate Cancer Cells. Molecular Cancer Research: MCR. 2019; 17: 2480–2491. https://doi.org/10.1158/1541-7786.MCR-19-0654
[68] Geiller HEB, Harvey A, Jones RE, Grimstead JW, Cleal K, Hendrickson EA, et al. ATRX modulates the escape from a telomere crisis. Plos Genetics. 2022; 18: e1010485. https://doi.org/10.1371/journal.pgen.1010485
[69] Taylor WR, Stark GR. Regulation of the G2/M transition by p53. Oncogene. 2001; 20: 1803–1815. https://doi.org/10.1038/sj.onc.1204252
[70] Stark GR, Taylor WR. Control of the G2/M transition. Molecular Biotechnology. 2006; 32: 227–248. https://doi.org/10.1385/MB:32:3:227